Gimbal Torque and Coupling Torque of Six Degrees of Freedom Magnetically Suspended Yaw Gimbal

***Abstract*—When the three-axis intertially stabilized platform (ISP) realizes the fast response of yaw gimbal, coupling torques among three gimbals cause negative influence on the attitude stabilization precision of yaw gimbal which supports the imaging payloads. Therefore, the gimbal torque of six degrees of freedom (DOFs) yaw gimbal with the magnetic suspension system is used to compensate coupling toques acting on it in this article. The dynamics models of yaw gimbal and three-axis ISP are developed, and then coupling torques among three gimbals are analyzed, it varies with motion states of the base plate. Moreover, the characteristics about gimbal torque generated by the magnetic suspension system are studied, it can accurately track the control input of magnetic suspended system. Finally, experimental results indicate that the gimbal torque of magnetic suspension system can effectively compensate coupling torques acting on the yaw gimbal, so the attitude stabilization precision of yaw gimbal is improved.**

***Index Terms*—magnetic suspension system; attitude stabilization precision; coupling torque; gimbal torque.**

1. Introduction

In the airborne remote sensing and imaging system such as electro-optical sensor and laser beam, disturbances caused by aircraft's motions including shift, vibration and rotation directly affect the control precision of airborne remote sensing and imaging system, so the resolution of image is affected [1]. Therefore, in order to achieve the high resolution image, the airborne ISP was used to stabilize and point a broad array of sensing and imaging system, and it could hold the line of sight of the imaging sensor relative to the inertial coordinate [2-4]. However, those normal ISP systems used mechanical bearings and gears to support gimbals, so disturbances of external gimbals could be transmitted to the internal gimbal because of the friction, manufacturing error, assembly misalignments of mechanical bearings and gears. In addition, the unavoidable coupling effect among three gimbals generates disturbances on the control precisions of gimbals in the three-axis ISP， and the coupling effect will be intensified by the motions of base plate and gimbals.

In order to improve the control precisions of gimbals in the three-axis ISP, researches are focused on two sides—novel supporting structure and advanced control method. In the one hand, the magnetic suspension system with active magnetic bearing (AMB) was used to suspend the yaw gimbal and isolate disturbances of external gimbals (roll gimbal and pitch gimbal) in the three-axis ISP [5]. In this magnetically suspended yaw gimbal, the

rotor part of yaw gimbal is levitated by the magnetic suspension system, and the axial and radial displacements of yaw gimbal are actively controllable by regulating the control current of AMBs based on the displacement feedback [6-9]. Moreover, the magnetic suspension system in magnetically suspended flywheel could generate gimbal torque by controlling the tilting of rotor part, and the gimbal torques are promising to generate control torque for the suspended gimbals [10].

On the other hand, the control method is the research focus of suppressing coupling disturbances among three gimbals in the three-axis ISP. The coupling effect in a maglev dual-stage ISP was analyzed based on frequency-domain analysis including disturbance rejection, fine stage saturation and coarse stage structural resonance suppression [7], and the simulation about single input single output (SISO) control loop of gimbal was conducted. The literature [11] analyzed the coupling effect among three gimbals in the three-axis ISP, and the feedback linearization was applied to linearize the coupling terms. Experimental results indicated that the coupling terms among three gimbals negatively affected the attitude stabilization precisions of three gimbals. Therefore, the decoupling control was used to mitigate the coupling disturbance in a differential cable driving ISP [12]. The decoupling controller based on the feed-forward compensation was applied, and experimental results showed that the decoupling control could effectively suppress coupling disturbances [13, 14]. Moreover, the proportional–integral–derivative (PID) and intelligent PID control were widely applied in the control of three-axis ISP [15, 16]. In order to achieve higher control precision, other intelligent control methods such as fuzzy control [17-19], sliding mode control [18, 20], adaptive-based composite control [21-23], feed-forward control [24, 25], disturbance observer [26], H_∞ control [27, 28] and adaptive control based on neural network [29-32] were introduced into the control engineering of three-axis ISP too. However, the design and realization of those control methods are complex, even some kinds of control methods are hard to be implemented in practical control engineering.

Compared to the three-axis ISP consisting of three mechanical gimbals, even though disturbance torques caused by gimbal's friction can be mitigated in the yaw gimbal suspended by the magnetic suspension system, coupling torques among three gimbals still exist and affect the attitude stabilization precision of yaw gimbal. In addition, the yaw gimbal with magnetic suspension system has five more DOFs than the mechanical gimbal, so the gimbal torques are generated by controlling the rotations of yaw gimbal around other two non-principal inertial axes. Therefore, the suppress method for coupling torques and the control method of gimbal torque are worthy of being researched in this six DOFs yaw gimbal.

In this article, the gimbal torque is used to minimize the coupling torque acting on the yaw gimbal by

controlling its tilting motion. The dynamics of yaw gimbal with magnetic suspension system is studied, it has five more controllable DOFs than the mechanical gimbal. The characteristics of coupling torque and gimbal torque are analyzed, and the gimbal torques generated by magnetic suspension system are applied to suppress coupling torque acting on the yaw gimbal. This work presents a more implementable way to attenuate the coupling torque in the three-axis ISP, it not only minimize the gimbal's friction in the mechanical gimbal, but also attenuate the coupling torque acting on the yaw gimbal.

2. Modeling of Gimbal Dynamics

2.1. Structure of Three-axis ISP

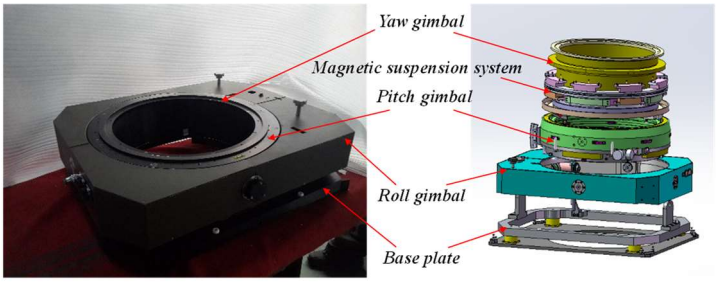

Fig. 1. The prototype and structure of three-axis ISP.

As illustrated in Fig. 1, the three-axis ISP has five parts—the base plate, the roll gimbal, the pitch gimbal, the magnetic suspension system and the yaw gimbal. The base plate is used to connect carriers (airplane, ship, vehicle and swaying platform) with the three-axis ISP. The roll gimbal is the external gimbal of three-axis ISP, and it only rotate around y_y axis of three-axis ISP. The pitch gimbal only rotate around x_y axis of three-axis ISP, and it is the middle gimbal. The magnetic suspension system suspends the rotor part of yaw gimbal, the stator part of magnetic suspension system is mounted on the bottom-end of yaw gimbal and the top-end of pitch gimbal, and the rotor part of magnetic suspension system is fixed on the yaw gimbal. The magnetic suspension system can control yaw gimbal's motions on five DOFs including translations on three axes and rotations around two radial axes, and the torque motor controls yaw gimbal's rotation around z_y axis of three-axis ISP. Payloads such as the positioning and orientation system (POS) are mounted on the yaw gimbal.

2.2. Gimbal Dynamics of Three-axis ISP

The whole coordinate system of three-axis ISP is illustrated in Fig. 2, and it is separated into three single gimbal coordinates. $Ox_yy_yz_y$ is the coordinate of yaw gimbal, $Ox_py_pz_p$ is the coordinate of pitch gimbal, $Ox_ry_rz_r$ is the coordinate of roll gimbal, and $Ox_by_bz_b$ is the coordinate of base plate. In addition, θ_p^y is the relative rotational angle of yaw gimbal around pitch gimbal, θ_r^p is the relative rotational angle of pitch gimbal around roll gimbal, and θ_b^r is the relative rotational angle of roll gimbal around base plate, respectively. ω_p^y is the relative angular velocity of yaw gimbal around pitch gimbal, ω_r^p is the relative angular velocity of pitch gimbal around roll gimbal ,

and ω_b^r is the relative angular velocity of roll gimbal around the base plate, separately.

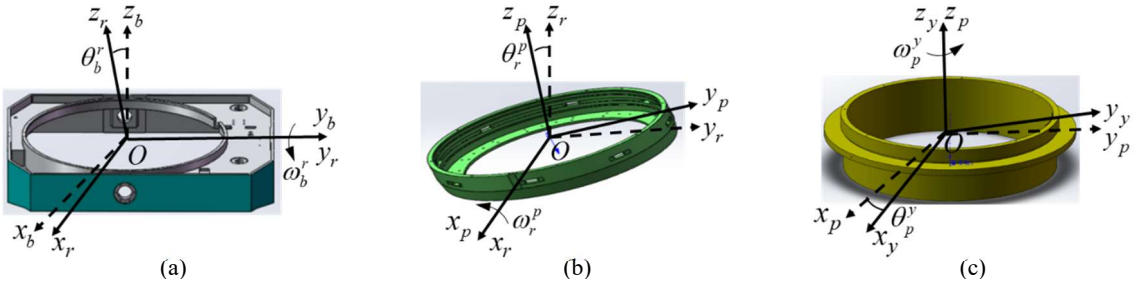

Fig. 2. Three coordinates of three-axis ISP, (a) coordinate of yaw gimbal, (b) coordinate of pitch gimbal, (c) coordinate of roll gimbal.

Given that the coordinate of base plate is the inertial coordinate, angular velocities of three gimbals are expressed as following,

$$\begin{cases} \boldsymbol{\omega}_r = C_b^r \boldsymbol{\omega}_b + (0 \quad \omega_b^r \quad 0)^T \\ \boldsymbol{\omega}_p = C_r^p C_b^r \boldsymbol{\omega}_b + C_r^p (0 \quad \omega_b^r \quad 0)^T + (\omega_r^p \quad 0 \quad 0)^T \\ \boldsymbol{\omega}_y = C_p^y C_r^p C_b^r \boldsymbol{\omega}_b + C_p^y C_r^p (0 \quad \omega_b^r \quad 0)^T + C_p^y (\omega_r^p \quad 0 \quad 0)^T + (0 \quad 0 \quad \omega_p^y)^T \end{cases} \tag{1}$$

where $\boldsymbol{\omega_b}=[\omega_{bx}\ \omega_{by}\ \omega_{bz}]^T$ are angular velocities of base plate relative to the inertial coordinate, $\boldsymbol{\omega_r}=[\omega_{rx}\ \omega_{ry}\ \omega_{rz}]^T$ are angular velocities of roll gimbal relative to the inertial coordinate, $\boldsymbol{\omega_p}=[\omega_{px}\ \omega_{py}\ \omega_{pz}]^T$ are angular velocities of pitch gimbal relative to the inertial coordinate, $\boldsymbol{\omega_y}=[\omega_{yx}\ \omega_{yy}\ \omega_{yz}]^T$ are angular velocities of yaw gimbal relative to the inertial coordinate. According to Appendix 1, the angular velocity of yaw gimbal around the principal axis z_y can be expressed into

$$\omega_{yz} = \omega_{bx} cos\theta_r^p \sin\theta_b^r - \omega_{by} \sin\theta_r^p + \omega_{bz} cos\theta_r^p \cos\theta_b^r - \omega_b^r \sin\theta_r^p + \omega_p^y \tag{2}$$

2.3. Rotational Dynamics of Yaw Gimbal

Given three gimbals in the three-axis ISP are symmetric structure and rigid body, according to the Newton-Euler rotational equation, the dynamic function of yaw gimbal can be written as following

$$\boldsymbol{T}_y = \boldsymbol{J}_y \dot{\boldsymbol{\omega}}_y + \boldsymbol{\omega}_y \times \boldsymbol{J}_y \boldsymbol{\omega}_y \tag{3}$$

Based on Appendix 2, the gimbal function of yaw gimbal around z_y axis can expressed into

$$T_{yz} = J_{yz}\dot{\omega}_{yz} - J_{yz}(\omega_{px}\omega_{ry}\cos\theta_{px} + \omega_{px}\omega_{rz}\sin\theta_{px}) + J_{yz}(-\omega_{ry}\sin\theta_{px} + \dot{\omega}_{rz}\cos\theta_{px}) \tag{4}$$

In general, for the yaw gimbal supported by mechanical bearings, it only rotates z_y axis in the three-axis ISP, and motions on other five DOFs are restricted by mechanical bearings and gears. However, the coupling torques T_{yy} and T_{yx} as shown in Appendix 2 will affect rotations of yaw gimbal around radial axes, and the stabilization precision of yaw gimbal along radial axes will be affected. Consequently, the control precision of yaw gimbal will be affected by coupling torques which vary with the rotations of base plate, the pitch gimbal and the roll gimbal. Therefore, the six DOFs yaw gimbal with magnetic suspension system is applied to suppress the coupling torque acting on yaw gimbal through controlling the tilting motion of yaw gimbal, and then stabilization precision of yaw

gimbal is improved.

3. Characteristics of Magnetic Suspension System

The yaw gimbal is levitated by the radial and axial suspension system. The radial suspension system generates suspension force to control the radial translation of yaw gimbal. The axial suspension system generates suspension force to control the axial translation, and also generates gimbal torque.

3.1. Radial Magnetic Suspension System

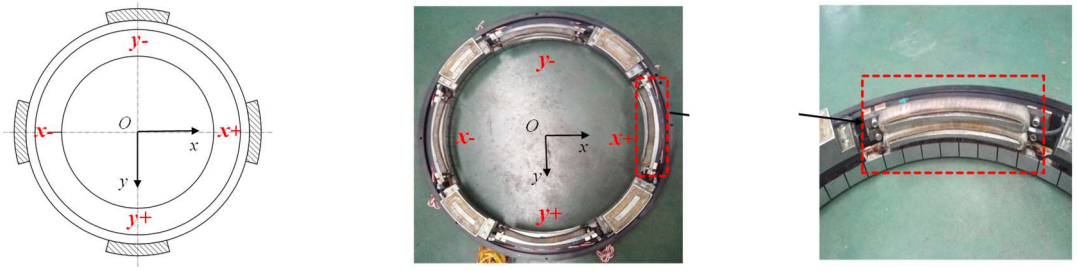

(a) (b) (c)

Fig. 3. Radial suspension system, (a) alignment of radial AMBs along *x*/*y* axes, (b) prototype of radial AMBs, (c) single-pole radial AMB in *x*+ direction.

As illustrated in Fig. 3, the radial suspension system contains two pairs of radial AMBs. One pair of radial AMBs control the translation of yaw gimbal in *x* axis, and another pair of radial AMBs control the translation of yaw gimbal in *y* axis. The difference between the suspension force f_{x+} in *x*+ direction and the suspension force f_{x-} in *x*- direction can realize the active control of yaw gimbal.

The resultant suspension forces in *x* axis and *y* axis can be expressed as follows, respectively,

$$\begin{cases} f_x = f_{x+} - f_{x-} \\ f_y = f_{y+} - f_{y-} \end{cases} \tag{5}$$

Furthermore, the suspension forces are expressed in terms of control current and displacement as follows,

$$\begin{cases} f_x = k_{ix} i_x - k_{dx} d_x \\ f_y = k_{iy} i_y - k_{dy} d_y \end{cases} \tag{6}$$

where k_{ix} is the current stiffness in *x* axis, k_{dx} is the displacement stiffness in *x* axis, k_{iy} is the current stiffness in *y* axis, k_{dy} is the displacement stiffness in *y* axis.

The relationship between the radial suspension force and the control current is shown in Fig. 4(a) when the radial displacement is -0.1mm, 0 and 0.1mm, respectively. The diagram of measured suspension force versus the control current is depicted in Fig. 5(a). The calculated and measured results indicate that the radial suspension force is linear to the control current and displacement within the vicinity of the radial equilibrium point, the radial current stiffness is 290*N*/*A*. The relationship between the radial suspension force and the radial displacement is plotted in Fig. 4(b) when the control current is -0.1A, 0 and 0.1A, and the measured result of radial suspension force versus the radial displacement is shown in Fig. 5(b). The radial displacement stiffness is -450*N*/*mm*.

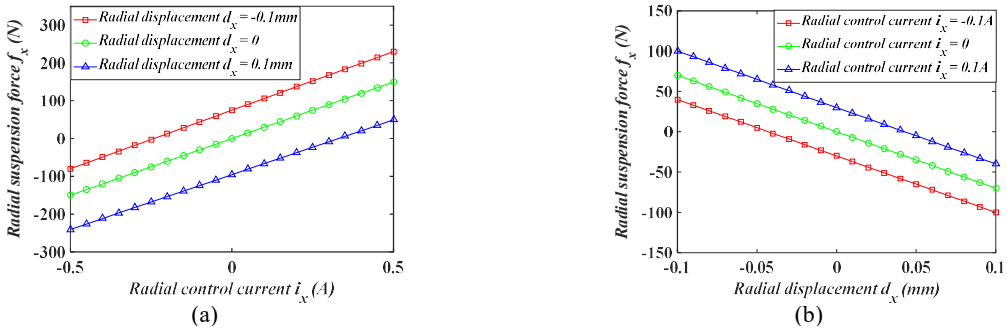

(a) (b)

Fig. 4. Radial suspension force, (a) radial suspension force f_x versus radial control current i_x, (b) radial suspension force f_x versus radial control displacement d_x.

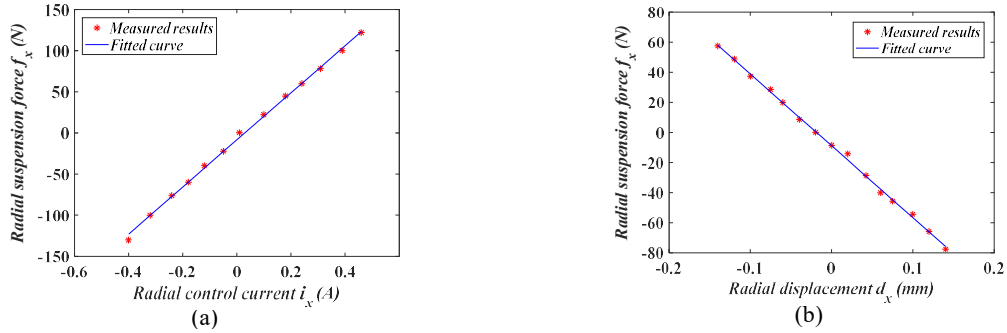

(a) (b)

Fig. 5. Measured results of radial suspension force, (a) radial suspension force f_x versus radial control current i_x, (b) radial suspension force f_x versus radial control displacement d_x.

3.2. Axial Magnetic Suspension System

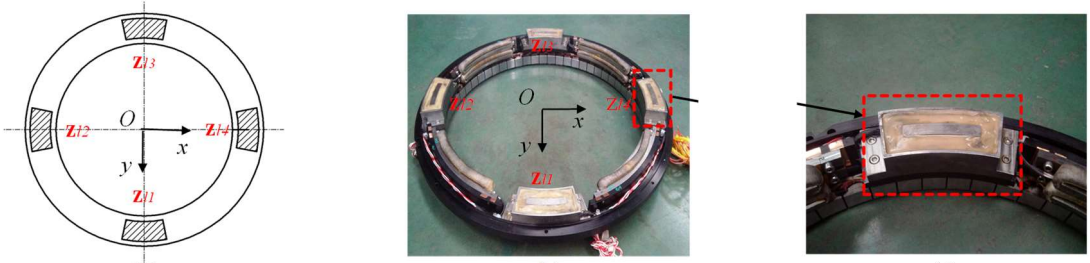

(a) (b) (c)

Fig. 6. Axial suspension system at low-end, (a) alignment of axial AMBs at low-end, (b) prototype of axial AMB at low-end, (c) single axial AMB at low-end.

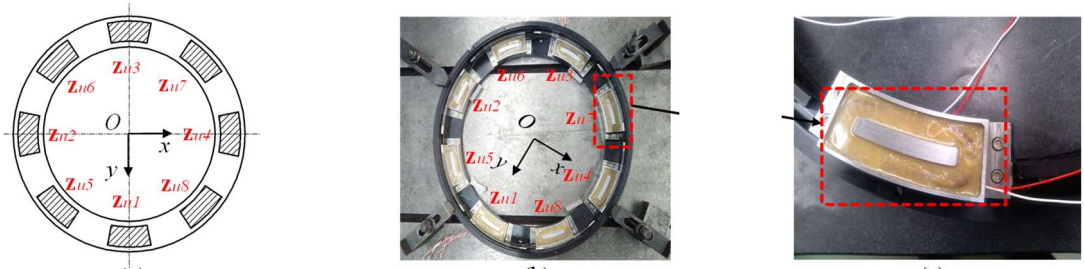

(a) (b) (c)

Fig. 7. Axial suspension system at up-end, (a) alignment of axial AMBs at up-end, (b) prototype of axial AMB at up-end, (c) single axial AMB at up-end.

The axial suspension system in Fig. 6 and Fig. 7 includes four AMBs at low-end and eight AMBs at up-end. Four pairs of axial AMBs (four AMBs z_{u1}, z_{u2}, z_{u3} and z_{u4} at up-end, four AMBs z_{l1}, z_{l2}, z_{l3} and z_{l4} at low-end) control the translation of yaw gimbal in z axis. Other four AMBs z_{u5}, z_{u6}, z_{u7} and z_{u8} at up-end generates gimbal torques by

controlling the tilting of yaw gimbal around radial axes.

The single-pole axial AMB at up-end is same as that at low-end, resultant suspension force in z axis is

$$f_z = 4 \times (f_{zu1} - f_{zl1}) \tag{7}$$

The linearized suspension force in z axis can be written into

$$f_z = k_{iz} i_z - k_{dz} d_z \tag{8}$$

where k_{iz} is the axial current stiffness, k_{dz} is the axial displacement stiffness.

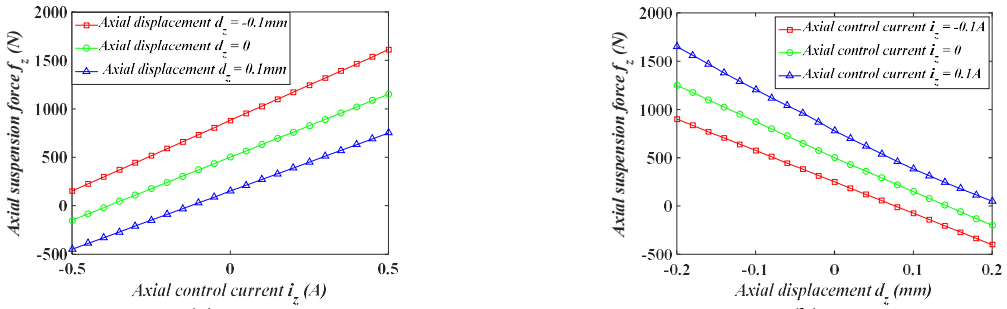

(a) (b)

Fig. 8. Axial suspension force, (a) axial suspension force f_z versus axial control current i_z, (b) axial suspension force f_z versus axial control displacement d_z.

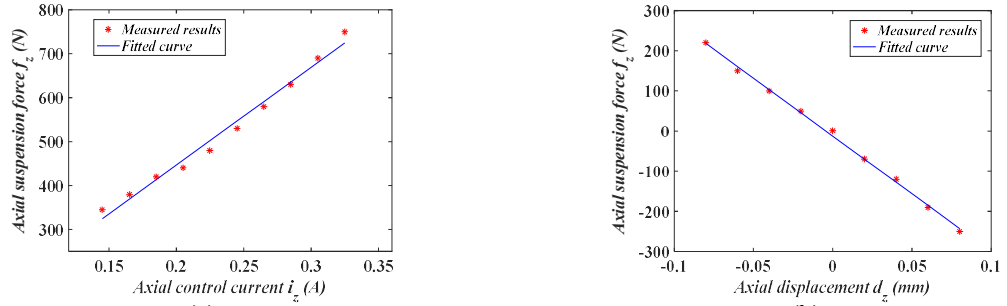

(a) (b)

Fig. 9. Measured result of axial suspension force, (a) axial suspension force f_z versus axial control current i_z, (b) axial suspension force f_z versus axial control displacement d_z.

When the yaw gimbal is suspended at the radial equilibrium point, and relationship between axial suspension force f_z and axial control displacement d_z is shown in Fig. 8(a). The relationship between axial suspension force f_z and axial control current i_z is illustrated in Fig. 8(b). The measured results of axial suspension force are plotted in Fig. 9, the axial current stiffness is 2222N/A, and the axial displacement stiffness is -2883N/mm.

3.3. Equation of Motion of Yaw Gimbal

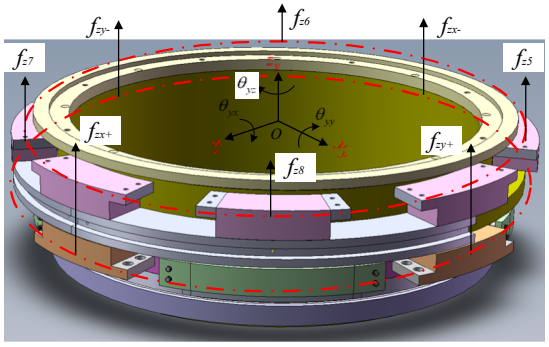

Fig. 10. Forces acting on the yaw gimbal.

The forces (tilting control force and suspension control force) acting on the yaw gimbal are illustrated in Fig. 10. f_{zx+}, f_{zx-}, f_{zy+} and f_{zy-} are suspension forces generated by four pairs of axial AMBs to control the axial suspension of yaw gimbal. f_{z5} and f_{z6}, f_{z7} and f_{z8} are suspension forces to generate gimbal torques around radial axes. For the yaw gimbal, the equations of motion with six DOFs are

$$\begin{cases} m\ddot{x} = f_x \\ m\ddot{y} = f_y \\ m\ddot{z} = f_z - mg \\ J_{yy}\ddot{\theta}_{yy} + J_{yz}\dot{\theta}_{yz}\dot{\theta}_{yx} = T_{yy} + T_{gy} \\ J_{yx}\ddot{\theta}_{yx} - J_{yz}\dot{\theta}_{yz}\dot{\theta}_{yy} = T_{yx} + T_{gx} \\ J_{yz}\ddot{\theta}_{yz} = T_{my} \end{cases} \tag{9}$$

where J_{yx}, J_{yy} and J_{yz} is the moment of inertia around x_y axis, y_y axis and z_y axis of yaw gimbal, respectively. T_{my} is the driving moment of yaw gimbal motor. θ_{yx} is the titling angle around x_y axis, θ_{yy} is the tilting angle around y_y axis, θ_{yz} is the rotational angle around z_y axis. T_{gy} is the gimbal torque around y_y axis, T_{gx} is the gimbal torque around x_y axis.

3.4. Gimbal Torque of Magnetic Suspension System

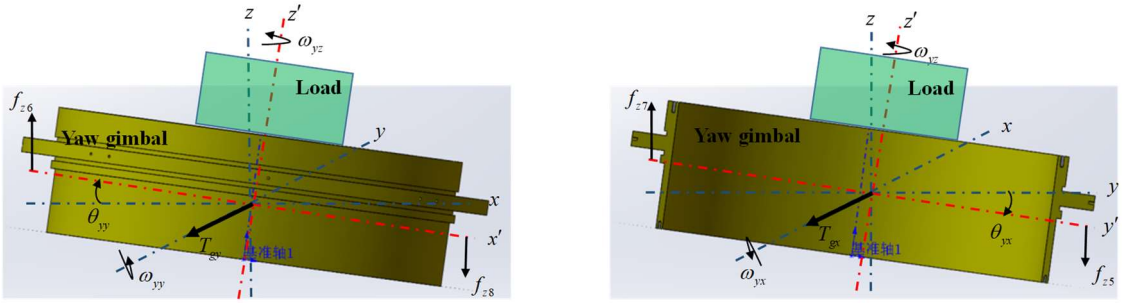

(a) (b)

Fig. 11. Titling motions of yaw gimbal around radial axes, (a) tilting of yaw gimbal around x_y axis, (b) tilting of yaw gimbal around y_y axis.

As illustrated in Fig. 11, the tilting of yaw gimbal around x_y axis and y_y axis are controlled by gimbal torques T_{gy} and T_{gx} generated by two pairs of axial AMBs at up-end, respectively. The arm length of suspension force is l. Gimbal torques can be expressed as

$$\begin{cases} T_{gy} = (f_{z6} - f_{z8}) \times l \\ T_{gx} = (f_{z7} - f_{z5}) \times l \end{cases} \tag{10}$$

The tilting control forces of magnetic suspension system are

$$\begin{cases} f_{z6} = k_{iz}i_{z6} - k_{dz}d_{z6} \\ f_{z8} = k_{iz}i_{z8} - k_{dz}d_{z8} \\ f_{z7} = k_{iz}i_{z7} - k_{dz}d_{z7} \\ f_{z5} = k_{iz}i_{z5} - k_{dz}d_{z5} \end{cases} \tag{11}$$

The translational displacement in z_y axis can be measured by axial displacement sensors, and the relationship

between the tilting angle and the axial displacement is

$$\begin{cases} d_{z6} - d_{z8} = l\sin\theta_{yy} \\ d_{z7} - d_{z5} = l\sin\theta_{yx} \end{cases} \tag{12}$$

The tilting control forces of magnetic suspension system are

$$\begin{cases} f_{z6} - f_{z8} = k_{iz}\Delta i - k_{dz}l\sin\theta_{yy} \\ f_{z7} - f_{z5} = k_{iz}\Delta i - k_{dz}l\sin\theta_{yx} \end{cases} \tag{13}$$

Consequently, gimbal torques of magnetic suspension system are

$$\begin{cases} T_{gy} = (k_{iz}\Delta i - k_{dz}l\sin\theta_{yy})l \\ T_{gx} = (k_{iz}\Delta i - k_{dz}l\sin\theta_{yx})l \end{cases} \tag{14}$$

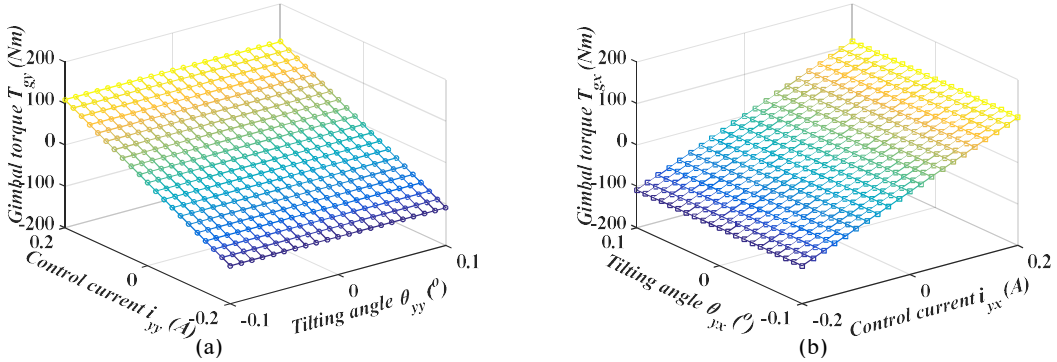

Fig. 12. Gimbal torques generated by magnetic suspension system, (a) relationship among gimbal torque T_{gy} around y_y axis, control current i_{yy} and tilting angle θ_{gy}, (b) relationship among gimbal torque T_{gy} around x_y axis, control current i_{yx} and tilting angle θ_{gx}.

Therefore, gimbal torques of magnetic suspension system are actively controllable by regulating the suspension force of axial AMBs at up-end based on the displacement feedback. Moreover, the coupling torque impacting on yaw gimbal can be compensated by the gimbal torque of magnetic suspension system. As illustrated in Fig. 12, the gimbal torque of magnetic suspension system is proportional to the control current and the titling angle, the current stiffness of gimbal torque is 554*Nm/A*, and the angular stiffness of gimbal torque is -173*Nm/deg*.

4. Attenuation for Coupling Torque

4.1. Control Scheme of Yaw Gimbal

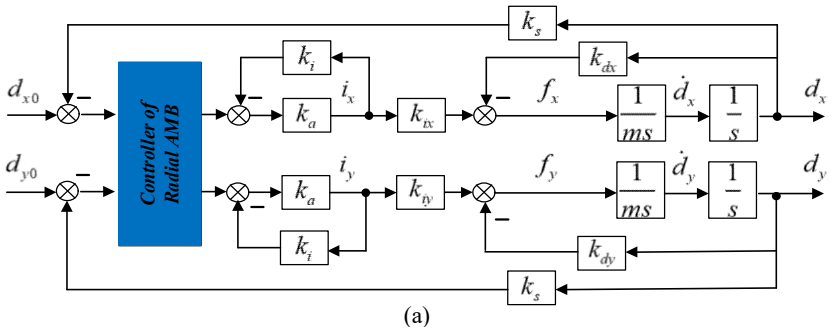

(a)

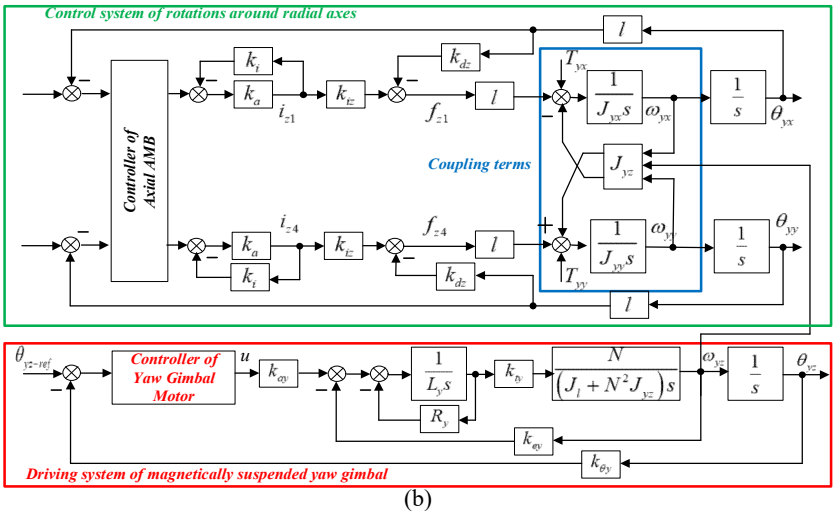

(b)

Fig. 13. Control scheme of yaw gimbal, (a) control scheme of magnetic suspension system, (b) control scheme of torque motor on yaw gimbal.

The whole control system of yaw gimbal is consisted of the control system of radial translations and the control system of rotations around three axes. In detail, the control loop of radial translation in Fig. 13(a) is independent from the control loop of rotation in Fig. 13(b). The radial displacements are measured by the displacement sensors and feedback to the control system, and then the error between the reference displacement and the feedback displacement will be transferred into the control current through AMB control unit (decentralized PD control) and voltage/current amplifier. Consequently, suspension forces are generated to make the rotor part of yaw gimbal suspend at equilibrium point. k_s is the sensitivity of displacement sensor, k_a is the amplification coefficient. The AMB control unit includes the proportional coefficient k_P and the derivative coefficient k_D.

Based on the displacement feedback of yaw gimbal, the control current is

$$i_x=(k_P+k_D s)k_a k_s \cdot d_x \tag{15}$$

Substitute Eq.(15) into Eq.(6), the suspension force in radial direction can be rewritten as

$$f_x=(k_{ix}k_P k_a k_s+k_{dx})\cdot d_x+k_{ix}k_D k_a k_s\cdot \dot{d}_x \tag{16}$$

Therefore, the transfer function of translational control system can be written as

$$G(s)=\frac{k_a k_s k_i k_D s+k_a k_s k_i k_P+k_d}{ms^2+k_a k_s k_i k_D s+k_a k_s k_i k_P+k_d} \tag{17}$$

For the rotational control loop shown in the red square diagram in Fig. 13(b), the rotation around z_y axis is driven by the torque motor. The rotations around radial axes in green square diagram are controlled by the axial AMBs at up-end, and coupling torques shown in blue square diagram are introduced when the yaw gimbal realizes fast maneuvering. Therefore, rotations around radial axes will generate the gimbal torque to compensate coupling torques acting on yaw gimbal. In detail, θ_{yz} is the rotational angle. u is the control voltage of torque motor. L_y is

the armature inductance. R_y is the armature resistance. k_{ty} is the torque coefficient. N is gear ratio. J_l is the inertia of moment of load, and k_{ey} is the back-EMF coefficient. The driving moment of torque motor is

$$T_{my} = \frac{k_{tt}}{L_y s + R_t}(u - k_{et}\dot{\theta}_{yz}) \tag{18}$$

The rotational function of yaw gimbal can be written as

$$J_{yz}\ddot{\theta}_{yz} = \frac{k_{ty}}{L_y s + R_t}(u - k_{et}\dot{\theta}_{yz}) \tag{19}$$

4.2. Experimental Setup

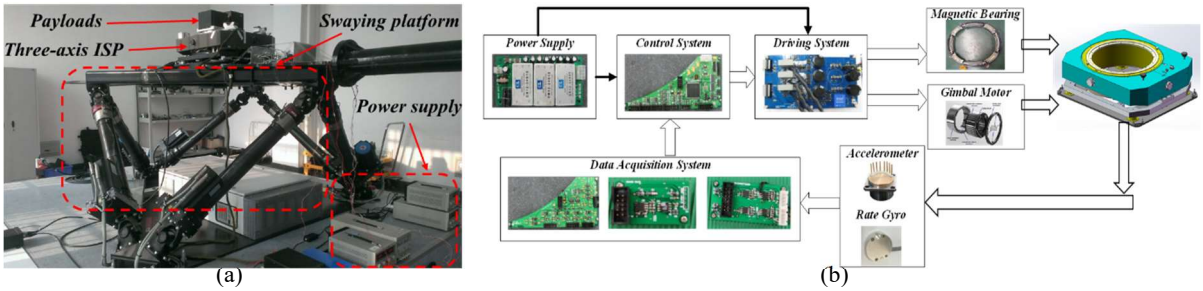

(a) (b)

Fig. 14. Experimental setup, (a) three-axis ISP and swaying platform system, (b) control system of the three-axis ISP.

Table 1. Parameters of experimental setup.

Parameter	Value	Unit
Radial current stiffness	k_{ix}=290	*N/A*
Radial displacement stiffness	k_{dx}=-450	*N/mm*
Axial current stiffness	k_{iz}=2222	*N/A*
Axial displacement stiffness	k_{dz}=-2883	*N/mm*
Current stiffness of gimbal torque	544	*Nm/A*
Angular stiffness of gimbal torque	-173	*Nm/deg*
Inertia of moment around *z* axis of yaw gimbal	J_{yz}=3.2	kgm^2
Inertia of moment around *x* axis of yaw gimbal	J_{yx}=2.4	kgm^2
Inertia of moment around *y* axis of yaw gimbal	J_{yy}=2.4	kgm^2
Arm length of suspension force	l=0.245	*m*
Sensitivity of displacement sensor	k_s=0.3	*V/mm*
Amplification coefficient	k_a=0.2	*A/V*
Motor torque constant	k_{ty}=0.4	*Nm/A*
Back EMF constant of torque motor	k_{ey}=0.4	*V/rad/s*

The whole experimental setup contains the swaying platform system, the three-axis ISP, the power supply system and the control system. The base plate of three-axis ISP is mounted on the swaying platform which outputs dynamic disturbance on the three-axis ISP to simulate the disturbance in the flight experiment. Moreover, the magnetic suspension system generates suspension forces to make the yaw gimbal suspend at the equilibrium point, and gimbal torques could compensate the coupling torques acting on yaw gimbal. The whole control unit based on a digital signal processor (DSP) TM320F28335 with 12-bit A/D convertor is embedded in the three-axis ISP. The data acquisition (DAQ) system is used to collect the displacement signal of yaw gimbal, the acceleration signal

and the attitude signal of three gimbals, and the sampling frequency is 20*KHz*. The driving system based on a pulse width modification (PWM) amplifier with 20*KHz* is used to drive the magnetic suspension system and three torque motors. The power supply system outputs voltage with 28*V*. Moreover, other parameters of experimental system are listed in Table 1.

4.3. Suspension Characteristics of Yaw Gimbal

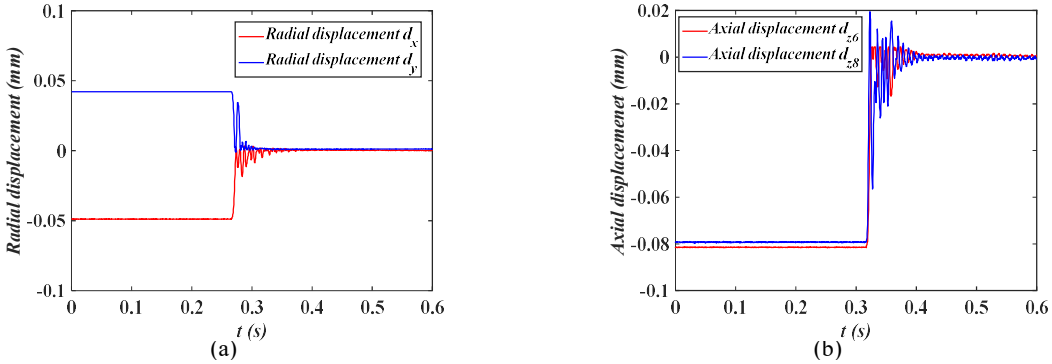

Fig. 15. Radial and axial suspension control of yaw gimbal, (a) radial displacement of yaw gimbal, (b) axial displacement of yaw gimbal.

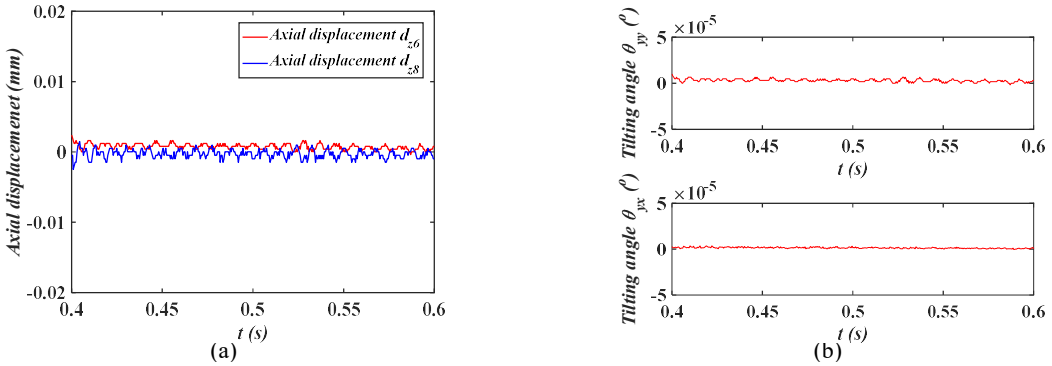

Fig. 16. Static suspension precision of yaw gimbal, (a) axial displacement precision, (b) axial angle precision.

This experiment is conducted to testify the suspension characteristics of magnetic suspension system. Fig. 15 indicates the suspension processes of yaw gimbal's rotor part in radial and axial directions. When radial displacements d_x and d_y equal to zero, the rotor part of yaw gimbal is stably suspended at the radial equilibrium point. When axial displacements d_{z6} and d_{z8} are zero, the rotor part of yaw gimbal is stably suspended at the axial equilibrium point. Fig. 16 shows the static suspension precision of yaw gimbal when it is suspended at the radial and axial equilibrium point. For the axial suspension precision in Fig. 16(a), the root mean square (RMS) is used to evaluate the stabilization precision, the smaller value of RMS is, the higher stabilization precision is. The RMS of displacement in x_y axis and y_y axis is 0.5μm and 0.4μm, respectively. The RMS of angle precision in z_y axis is 0.9μm. For the tilting precision of yaw gimbal, the RMS of θ_{yy} and θ_{yx} is 0.0039 and 0.0027 , respectively.

Table 2. Static suspension precision of yaw gimbal.

Suspension status	**Precisio**

Displacement precision in x_y axis	0.5μm
Displacement precision in y_y axis	0.4μm
Displacement precision in z_y axis	0.9μm
Tilting angle precision around y_y axis	0.0039
Tilting angle precision around x_y axis	0.0027

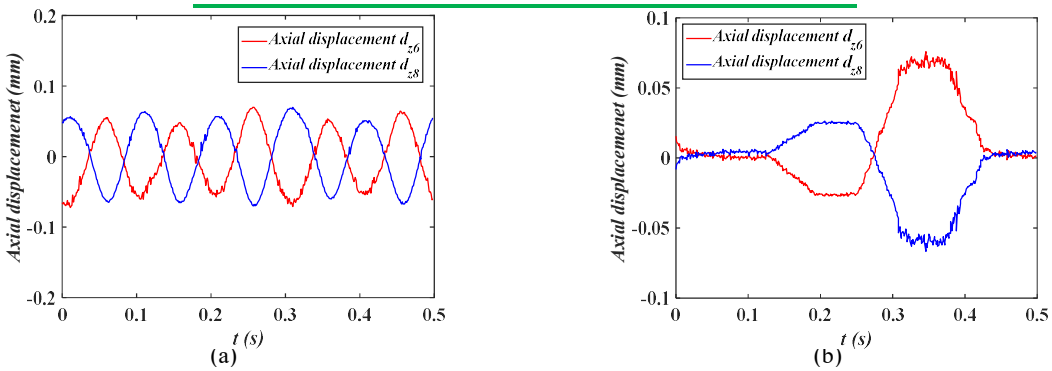

Fig. 17. Tilting of yaw gimbal around radial axis, (a) sinusoidal tilting of yaw gimbal, (b) step tilting of yaw gimbal.

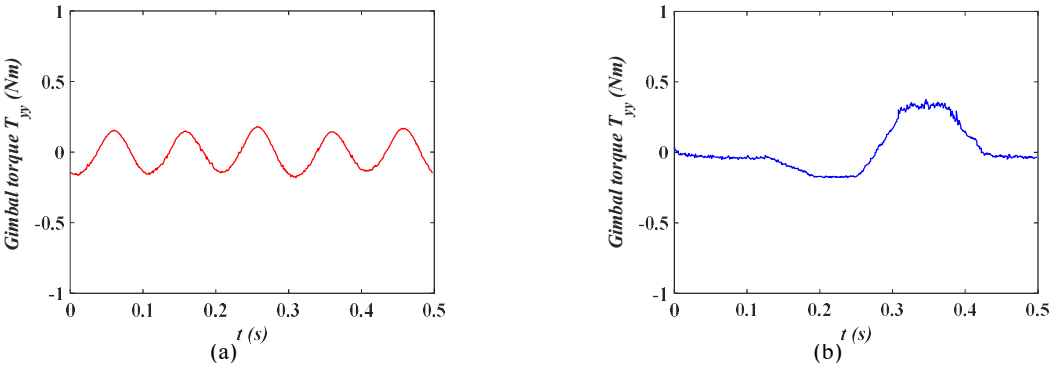

Fig. 18. Gimbal torque generated by magnetic suspension system, (a) gimbal torque of sinusoidal tilting, (b) gimbal torque of step tilting.

Moreover, the active controllability of magnetic suspension system is verified. The tilting of yaw gimbal is controllable by regulating suspension forces of axial AMBs z_{u5}, z_{u6}, z_{u7} and z_{u8} at up-end. The sinusoidal tilting of yaw gimbal is shown in Fig. 17(a), and the step tilting of yaw gimbal is illustrated in Fig. 17(b). Based on the tilting displacements of yaw gimbal, the gimbal torques generated by magnetic suspension system are plotted in Fig. 18, It indicates that the gimbal torque is controllable based on the tilting displacement of yaw gimbal, so the gimbal torque has a good performance on tracking the referring titling displacement.

The suspension experiment and tilting experiment verify the active controllability of magnetic suspension system, so it is implementable that gimbal torques can be used to suppress coupling torques acting on yaw gimbal.

4.4. *Coupling Torque Acting on Yaw Gimbal*

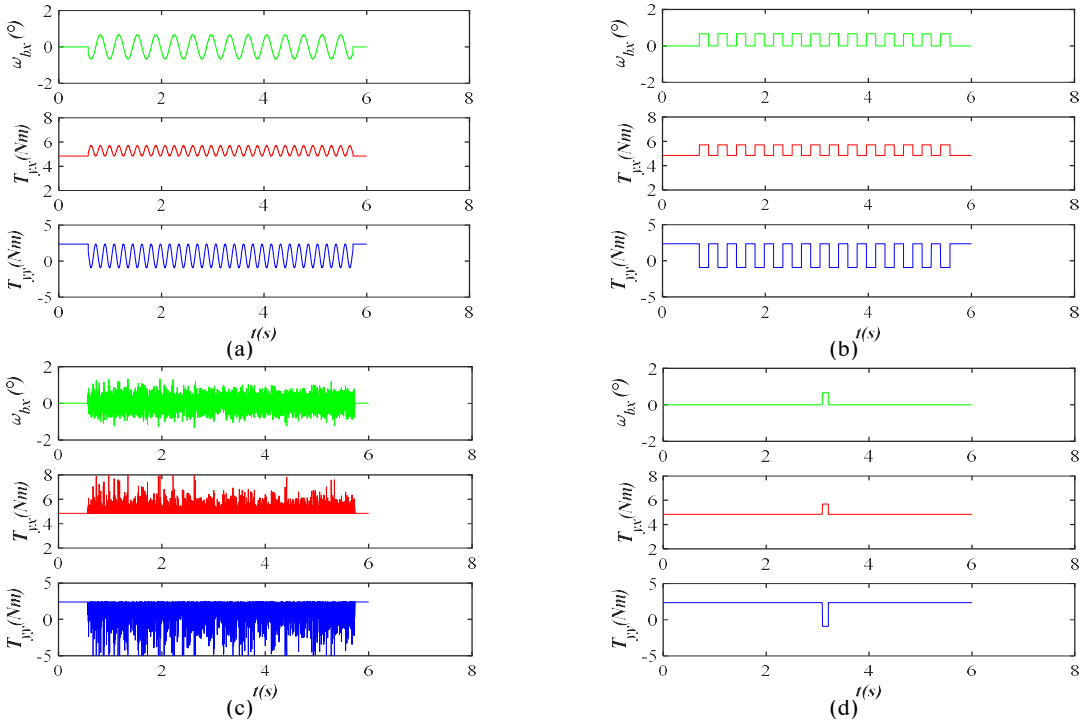

Fig. 19. Four types of coupling torque acting on yaw gimbal, (a) coupling torque of sinusoidal signal, (b) coupling torque of square signal, (c) coupling torque of random signal, (d) coupling torque of impulse signal.

This part is to validate influence of coupling torques acting on the yaw gimbal. Different signals are imposed on the base plate, so coupling torques acting on yaw gimbal will vary with the angular motions of base plate. In the practical flight experiment, the rotational range of pitch gimbal and roll gimbal is about [-5°, +5°], and the control range of yaw gimbal is about [-20°, +20°], so the rotational angle of base plate around x_b axis setts as 1°. As illustrated in Fig. 19, the green line is the angular displacement of base plate, the red line is the coupling torque T_{yx} around y_x axis, and the blue line is the coupling torque T_{yy} around y_y axis. Firstly, a sinusoidal signal $sin(0.4\pi t)$ is imposed on the base plate, coupling torques among three gimbals are shown in Fig. 19(a). When the base plate outputs continuous square signal with amplitude 1° and duty ratio 50% as shown in Fig. 19(b), coupling torques also change with the angular displacement of base plate. Moreover, the coupling torque for the random signal is shown in Fig. 19(c), coupling torque has a bias values, T_{yx} is greater than the bias value, but T_{yy} is smaller than the bias value. Finally, the impulse response of coupling torque is plotted in Fig. 19(d), the coupling torque also has an impulse response. The response amplitude of coupling torque T_{yy} around y_y axis is always greater than the coupling torque T_{yx} around y_x axis. Consequently, coupling torques acting on yaw gimbal vary with the angular displacement of base plate, and the coupling toque T_{yy} around y_y axis has a more important role on the attitude stabilization precision of yaw gimbal.

4.5. Attenuating Effect of Gimbal Torque

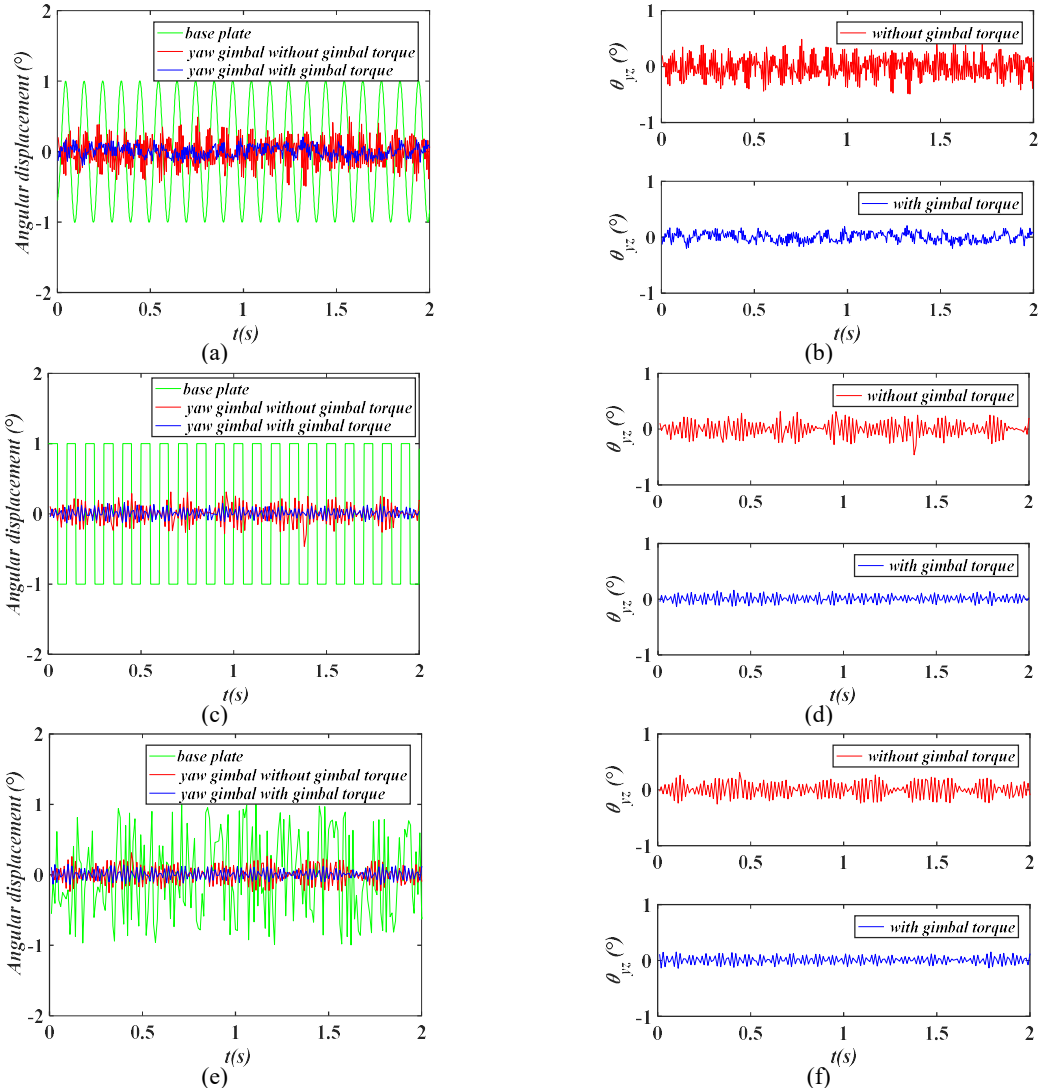

Fig. 20. Attitude stabilization precision of yaw gimbal for different disturbances, (a) attitude stabilization precision of yaw gimbal for sinusoidal signal, (b) comparison between attitude stabilization precision of yaw gimbal for sinusoidal signal with and without gimbal torque, (c) attitude stabilization precision of yaw gimbal for square signal, (d) comparison between attitude stabilization precision of yaw gimbal for square signal with and without gimbal torque, (e) attitude stabilization precision of yaw gimbal with random signal, (f) comparison between attitude stabilization precision of yaw gimbal for random signal with and without gimbal torque.

In this experiment, the attenuating ability for coupling torques acting on yaw gimbal is validated. As illustrated in Fig. 20, the attitude stabilization precisions of yaw gimbal with different disturbances are measured, the green line is the angular displacement of base plate, the red line is the attitude stabilization precision of yaw gimbal without gimbal torque compensation, and the blue line is the attitude stabilization precision of yaw gimbal with gimbal torque compensation. The RMS of attitude stabilization precision is the evaluation index for the control precision of yaw gimbal.

For the dynamic base plate with the sinusoidal signal, the attitude stabilization precision of yaw gimbal is

plotted in Fig. 20(a), the RMS of attitude stabilization precision without gimbal torque compensation is 0.2134°. The attitude stabilization precision with gimbal torque compensation is 0.0828°. In addition, as illustrated in Fig. 20(c), the base plate tilts with a square signal. The attitude stabilization precision of yaw gimbal without gimbal torque compensation is 0.1562°, and the attitude stabilization precision with gimbal torque compensation is reduced to 0.0725°. Moreover, the attitude suspension precision of yaw gimbal with the random disturbance is shown in Fig. 20(e). The attitude suspension precision without gimbal torque compensation is 0.1355°. When the gimbal torque is used, the RMS of attitude suspension precision is decreased to 0.0791°.

Table 3. Suspension precision of yaw gimbal.

	Attitude suspension precision		
	Sinusoidal disturbance	Square disturbance	Random disturbance
Without compensation	0.2134°	0.1562°	0.1355°
With compensation	0.0828°	0.0725°	0.0791°
Relative reduction	61.2%	63.6%	41.6%

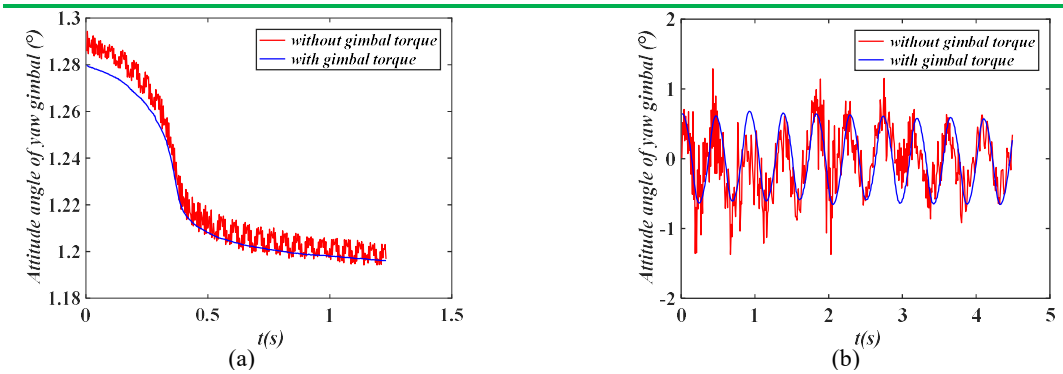

Fig. 21. Rotation control of yaw gimbal around z_y axis, (a) rotational angle of yaw gimbal for step input, (b) rotational angle of yaw gimbal for sinusoidal input.

Moreover, as illustrated in Fig. 21, the rotation of yaw gimbal around axial principal axis z_y axis is controlled by torque motor. When the angular displacement of yaw gimbal moves from 1.28° to 1.2° in Fig. 21 (a), the angular displacement of yaw gimbal without applying the gimbal torque contains high-frequency disturbance, and the deflection value is about 0.001°. The sinusoidal motion of yaw gimbal is shown in Fig. 21(b), the obvious disturbance is added on the angular displacement of yaw gimbal when the gimbal torque is not used.

Above all, experimental results indicate that gimbal torque generated by the magnetic suspension system can compensate coupling torques acting on yaw gimbal, so the attitude stabilization precision of yaw gimbal is improved.

5. Conclusion

This article introduces the three-axis ISP with a magnetic suspension system, and the yaw gimbal of three-

axis ISP is suspended by the magnetic suspension system. The suspension force of magnetic suspension system is linear to control current and displacement within the vicinity of equilibrium point. Furthermore, based on the dynamic equations of three-axis ISP, it is verified that coupling torques among three gimbals in the three-axis ISP cause negative influence on the attitude stabilization precision of yaw gimbal. Therefore, the gimbal torque of magnetic suspension system is used to compensate coupling torques acting on yaw gimbal by controlling its tilting motion. The experimental results indicate that the gimbal torque can effectively compensate the coupling torques acting on yaw gimbal, and then the attitude stabilization precision of yaw gimbal is improved.

Reference

[1] Z. Hurak and M. Rezac, "Image-based pointing and tracking for inertially stabilized airborne camera platform," *IEEE Transactions on Control Systems Technology,* vol. 20, no. 5, pp. 1146-1159, 2012.

[2] J. Hilkert, "Inertially stabilized platform technology concepts and principles," *IEEE Control Systems,* vol. 28, no. 1, pp. 26-46, 2008.

[3] H. G. Wang and T. C. Williams, "Strategic inertial navigation systems-high-accuracy inertially stabilized platforms for hostile environments. IEEE Control system Magazine," *Control Systems IEEE,* vol. 28, no. 1, pp. 65-85, 2008.

[4] M. K. Masten, "Inertially stabilized platforms for optical imaging systems," *IEEE Control Systems,* vol. 28, no. 1, pp. 47-64, 2008.

[5] J. Fang, C. Wang, and T. Wen, "Design and optimization of a radial hybrid magnetic bearing with separate poles for magnetically suspended inertially stabilized platform," *IEEE Transactions on Magnetics,* vol. 50, no. 5, pp. 1-11, 2014.

[6] Z. Lin and K. Liu, "Inertially stabilized line-of-sight control system using a magnetic bearing with vernier gimbaling capacity," in *SPIE/COS Photonics Asia*, 2014, pp. 92720Q-92720Q-11: International Society for Optics and Photonics.

[7] Z. Lin, K. Liu, Z. Li, and D. Zeng, "Coupling effect and control strategies of the maglev dual-stage inertially stabilization system based on frequency-domain analysis ☆," *Isa Transactions,* vol. 64, pp. 98-112, 2016.

[8] J. Sun, C. Wang, and L. Yun, "Designing and Experimental Verification of the Axial Hybrid Magnetic Bearing to Stabilization of a Magnetically Suspended Inertially Stabilized Platform," *IEEE/ASME Transactions on Mechatronics,* vol. 21, no. 6, pp. 2881-2891, 2016.

[9] Z. Lin, K. Liu, and Z. Wei, "Inertially stabilized platform for airborne remote sensing using magnetic bearings," *IEEE/ASME Transactions on Mechatronics,* vol. 21, no. 1, pp. 288-301, 2016.

[10] B. Xiang and J. Tang, "Suspension and titling of vernier-gimballing magnetically suspended flywheel with conical magnetic bearing and Lorentz magnetic bearing," *Mechatronics,* vol. 28, pp. 46-54, 2015.

[11] J. Fang, R. Yin, and X. Lei, "An adaptive decoupling control for three-axis gyro stabilized platform based on neural networks," *Mechatronics,* vol. 27, pp. 38-46, 2015.

[12] H. Liao, Y. Lu, S. Fan, and D. Fan, "Dynamics analysis and decoupling control for a differential cable drive inertially stabilized platform," *Proceedings of the Institution of Mechanical Engineers, Part I: Journal of Systems and Control Engineering,* vol. 229, no. 7, pp. 652-661, 2015.

[13] X. Zhou, G. Gong, J. Li, H. Zhang, and R. Yu, "Decoupling control for a three-axis inertially stabilized platform used for aerial remote sensing," *Transactions of the Institute of Measurement and Control,* vol. 37, no. 9,

pp. 1135-1145, 2015.
[14] X. Zhou, H. Zhang, and R. Yu, "Decoupling control for two-axis inertially stabilized platform based on an inverse system and internal model control," *Mechatronics,* vol. 24, no. 8, pp. 1203-1213, 2014.
[15] W. Ji, Q. Li, and B. Xu, "Design study of adaptive fuzzy PID controller for LOS stabilized system," in *Intelligent Systems Design and Applications, 2006. ISDA'06. Sixth International Conference on*, 2006, vol. 1, pp. 336-341: IEEE.
[16] Y. Zhang *et al.*, "Fuzzy-PID control for the position loop of aerial inertially stabilized platform," *Aerospace Science and Technology,* vol. 36, pp. 21-26, 2014.
[17] J. K. Moorty, R. Marathe, and H. Babu, "Fuzzy controller for line-of-sight stabilization systems," *Optical Engineering,* vol. 43, no. 6, pp. 1394-1400, 2004.
[18] H. Hong, P. Yun, C. Zhao, and Q. Wu, "The application research on fuzzy PI control arithmetic of photoelectric stabilized platform," in *Intelligent Systems and Applications, 2009. ISA 2009. International Workshop on*, 2009, pp. 1-5: IEEE.
[19] F.-J. Lin and P.-H. Shen, "Robust fuzzy neural network sliding-mode control for two-axis motion control system," *IEEE Transactions on Industrial Electronics,* vol. 53, no. 4, pp. 1209-1225, 2006.
[20] Y. B. Shtessel, "Decentralized sliding mode control in three-axis inertial platforms," *Journal of Guidance, Control, and Dynamics,* vol. 18, no. 4, pp. 773-781, 1995.
[21] Y. Zou and X. Lei, "A compound control method based on the adaptive neural network and sliding mode control for inertial stable platform," *Neurocomputing,* vol. 155, pp. 286-294, 2015.
[22] K. Tan, T. Lee, A. Mamun, M. Lee, and C. Khoh, "Composite control of a gyro mirror line-of-sight stabilization platform—design and auto-tuning," *ISA transactions,* vol. 40, no. 2, pp. 155-171, 2001.
[23] X. Lei, Y. Zou, and F. Dong, "A composite control method based on the adaptive RBFNN feedback control and the ESO for two-axis inertially stabilized platforms," *ISA transactions,* vol. 59, pp. 424-433, 2015.
[24] Q. Mu, G. Liu, M. Zhong, and Z. Chu, "Imbalance torque compensation for three-axis inertially stabilized platform using acceleration feedforward," in *Instrumentation and Control Technology (ISICT), 2012 8th IEEE International Symposium on*, 2012, pp. 157-160: IEEE.
[25] M. Řezáč and Z. Hurák, "Vibration rejection for inertially stabilized double gimbal platform using acceleration feedforward," in *Control Applications (CCA), 2011 IEEE International Conference on*, 2011, pp. 363-368: IEEE.
[26] J. Hilkert and B. Pautler, "A reduced-order disturbance observer applied to inertially stabilized line-of-sight control," in *Acquisition, Tracking, Pointing, and Laser Systems Technologies XXV*, 2011, vol. 8052, p. 80520H: International Society for Optics and Photonics.
[27] M. R. Darestani, A. A. Nikkhah, and A. K. Sedigh, "H∞/Predictive output control of a three-axis gyrostabilized platform," *Proceedings of the Institution of Mechanical Engineers, Part G: Journal of Aerospace Engineering,* vol. 228, no. 5, pp. 679-689, 2014.
[28] H. Khodadadi, M. Motlagh, and M. Gorji, "Robust control and modeling a 2-DOF Inertial Stabilized Platform," in *International Conference on Electrical*, 2011.
[29] T. Lee, S. Ge, and C. Wong, "Adaptive neural network feedback control of a passive line-of-sight stabilization system," *Mechatronics,* vol. 8, no. 8, pp. 887-903, 1998.
[30] J. F. Quindlen, G. Chowdhary, and J. P. How, "Hybrid model reference adaptive control for unmatched uncertainties," in *American Control Conference (ACC), 2015*, 2015, pp. 1125-1130: IEEE.
[31] K. C. Tan, T. H. Lee, E. F. Khor, and D. Ang, "Design and real-time implementation of a multivariable gyro-mirror line-of-sight stabilization platform," *Fuzzy Sets and Systems,* vol. 128, no. 1, pp. 81-93, 2002.
[32] D. Wang and J. Huang, "Neural network-based adaptive dynamic surface control for a class of uncertain

nonlinear systems in strict-feedback form," *IEEE Transactions on Neural Networks,* vol. 16, no. 1, pp. 195-202, 2005.

Appendix

Appendix.1

Three coordinate transformation matrices are

$$C_b^r=\begin{pmatrix}\cos\theta_b^r & 0 & -\sin\theta_b^r\\ 0 & 1 & 0\\ \sin\theta_b^r & 0 & \cos\theta_b^r\end{pmatrix},\quad C_r^p=\begin{pmatrix}1 & 0 & 0\\ 0 & \cos\theta_r^p & \sin\theta_r^p\\ 0 & -\sin\theta_r^p & \cos\theta_r^p\end{pmatrix},\quad C_p^y=\begin{pmatrix}\cos\theta_p^y & \sin\theta_p^y & 0\\ -\sin\theta_p^y & \cos\theta_p^y & 0\\ 0 & 0 & 1\end{pmatrix} \tag{a1.1}$$

Angular velocities of three gimbals are expressed as following,

$$\boldsymbol{\omega}_r=\begin{pmatrix}\omega_{bx}\cos\theta_b^r-\omega_{bz}\sin\theta_b^r\\ \omega_{by}+\omega_b^r\\ \omega_{bx}\cos\theta_b^r+\omega_{bz}\sin\theta_b^r\end{pmatrix} \tag{a1.2}$$

$$\boldsymbol{\omega}_p=\begin{pmatrix}\omega_{bx}\cos\theta_b^r-\omega_{bz}\sin\theta_b^r+\omega_r^p\\ \omega_{bx}\sin\theta_r^p\sin\theta_b^r+\omega_{by}\cos\theta_r^p+\omega_{bz}\sin\theta_r^p\cos\theta_b^r+\omega_b^r\cos\theta_r^p\\ \omega_{bx}\cos\theta_r^p\sin\theta_b^r-\omega_{by}\sin\theta_r^p+\omega_{bz}\cos\theta_r^p\cos\theta_b^r-\omega_b^r\sin\theta_r^p\end{pmatrix} \tag{a1.3}$$

$$\begin{aligned}\boldsymbol{\omega}_y=&\begin{pmatrix}\omega_{bx}\left(\sin\theta_p^y\sin\theta_r^p\sin\theta_b^r+\cos\theta_p^y\cos\theta_b^r\right)\\ \omega_{bx}\left(\cos\theta_p^y\sin\theta_r^p\sin\theta_b^r-\sin\theta_p^y\cos\theta_b^r\right)\\ \omega_{bx}cos\theta_r^p\sin\theta_b^r-\omega_{by}\sin\theta_r^p\end{pmatrix}+\begin{pmatrix}\omega_{by}\sin\theta_p^y\cos\theta_r^p\\ \omega_{by}\cos\theta_p^y\cos\theta_r^p\\ -\omega_{by}\sin\theta_r^p\end{pmatrix}\\ &+\begin{pmatrix}\omega_{bz}(sin\theta_p^y\sin\theta_r^p\cos\theta_b^r-\cos\theta_p^y\sin\theta_b^r)\\ -\omega_{bz}\left(\cos\theta_p^y\sin\theta_r^p\cos\theta_b^r+\sin\theta_p^y\sin\theta_b^r\right)\\ \omega_{bz}cos\theta_r^p\cos\theta_b^r\end{pmatrix}+\begin{pmatrix}\omega_b^r\sin\theta_p^y\cos\theta_r^p+\omega_r^p\cos\theta_p^y\\ \omega_b^r\cos\theta_p^y\cos\theta_r^p-\omega_r^p\sin\theta_p^y\\ -\omega_b^r\sin\theta_r^p+\omega_p^y\end{pmatrix}\end{aligned} \tag{a1.4}$$

Appendix.2

Assuming each gimbal of three-axis ISP is a symmetric structure and rigid body, according to the Newton-Euler rotational equation, the torques of gimbals are written as

$$\boldsymbol{T}=\boldsymbol{J}\dot{\boldsymbol{\omega}}+\boldsymbol{\omega}\times\boldsymbol{J}\boldsymbol{\omega} \tag{a2.1}$$

For roll gimbal, the torque acting on each axis is $\boldsymbol{T}_r=[T_{rx}\ T_{ry}\ T_{rz}]^T$, and

$$\begin{cases}T_{rx}=J_{rx}\dot{\omega}_{rx}-(J_{ry}-J_{rz})\omega_{ry}\omega_{rz}\\ T_{ry}=J_{ry}\dot{\omega}_{ry}-(J_{rx}-J_{rz})\omega_{rx}\omega_{rz}\\ T_{rz}=J_{rz}\dot{\omega}_{rz}-(J_{rx}-J_{ry})\omega_{rx}\omega_{ry}\end{cases} \tag{a2.2}$$

where J_{rx}, J_{ry} and J_{rz} are moments of inertia about three axes of roll gimbal, respectively.

For pitch gimbal, the torque acting on each axis is $\boldsymbol{T}_p=[T_{px}\ T_{py}\ T_{pz}]^T$, and

$$\begin{cases}T_{px}=J_{px}\left(\dot{\omega}_{rx}+\ddot{\theta}_{px}\right)-\left(J_{ry}-J_{rz}\right)\left(\omega_{rz}sin\theta_{px}+\omega_{ry}cos\theta_{px}\right)\left(\omega_{rz}cos\theta_{px}-\omega_{ry}sin\theta_{px}\right)\\ T_{py}=J_{py}\left[\left(\dot{\omega}_{ry}+\dot{\theta}_{px}\omega_{rz}\right)cos\theta_{px}-\left(\omega_{rz}+\dot{\theta}_{px}\omega_{ry}\right)sin\theta_{px}\right]-\left(J_{rx}-J_{rz}\right)\left(\omega_{rz}cos\theta_{px}-\omega_{ry}sin\theta_{px}\right)\left(\dot{\omega}_{rx}+\dot{\theta}_{px}\right)\\ T_{pz}=J_{pz}\left(-\dot{\omega}_{ry}sin\theta_{px}-\dot{\theta}_{px}\omega_{ry}cos\theta_{px}+\omega_{rz}cos\theta_{px}-\dot{\theta}_{px}\omega_{rz}sin\theta_{px}\right)\end{cases} \tag{a2.3}$$

where J_{px}, J_{py} and J_{pz} are moments of inertia about three axes of pitch gimbal, respectively.

For yaw gimbal, the torque acting on each axis is $\boldsymbol{T}_y=[T_{yx}\ T_{yy}\ T_{yz}]^T$, and

$$\begin{cases} T_{yx} = J_{yx}[(\dot{\omega}_{rx} + \ddot{\theta}_{px})\cos\theta_{yz} - \dot{\theta}_{yz}(\omega_{rx} + \dot{\theta}_{px})\sin\theta_{yz} + \dot{\theta}_{yz}(\omega_{ry}\cos\theta_{px} + \omega_{rz}\sin\theta_{px})\cos\theta_{yz} \\ +(\dot{\omega}_{ry}\cos\theta_{px} - \dot{\theta}_{px}\omega_{ry}\sin\theta_{px} + \dot{\omega}_{rz}\sin\theta_{px} + \dot{\theta}_{px}\omega_{rz}\cos\theta_{px})\sin\theta_{yz}] \\ -(J_{yy} - J_{yz})(\omega_{rz}\cos\theta_{px} - \omega_{ry}\sin\theta_{px} + \dot{\theta}_{yz})[(\omega_{rz}\sin\theta_{px} + \omega_{ry}\cos\theta_{px})\cos\theta_{yz} - (\omega_{rx} + \dot{\theta}_{yz})\sin\theta_{yz}] \\ T_{yy} = J_{yy}[-(\dot{\omega}_{rx} + \ddot{\theta}_{px})\sin\theta_{yz} - \dot{\theta}_{yz}(\omega_{rx} + \dot{\theta}_{px})\cos\theta_{yz} - \dot{\theta}_{yz}(\omega_{ry}\cos\theta_{px} + \omega_{rz}\sin\theta_{px})\sin\theta_{yz} \\ +(\dot{\omega}_{ry}\cos\theta_{px} - \dot{\theta}_{px}\omega_{ry}\sin\theta_{px} + \dot{\omega}_{rz}\sin\theta_{px} + \dot{\theta}_{px}\omega_{rz}\cos\theta_{px})\cos\theta_{yz}] \\ -(J_{yz} - J_{yx})(\omega_{rz}\cos\theta_{px} - \omega_{ry}\sin\theta_{px} + \dot{\theta}_{yz})[(\omega_{rz}\sin\theta_{px} + \omega_{ry}\cos\theta_{px})\sin\theta_{yz} + (\omega_{rx} + \dot{\theta}_{yz})\cos\theta_{yz}] \\ T_{yz} = J_{yz}(-\omega_{ry}\sin\theta_{px} - \dot{\theta}_{px}\omega_{ry}\cos\theta_{px} + \dot{\omega}_{rz}\cos\theta_{px} - \dot{\theta}_{px}\omega_{rz}\sin\theta_{px} + \ddot{\theta}_{yz}) \end{cases} \quad \text{(a2.5)}$$

where J_{yx}, J_{yy} and J_{yz} are moments of inertia about three axes of yaw gimbal, respectively.

In the three-axis ISP, pitch gimbal and roll gimbal only rotate around their rotational principal axes, so

$$\begin{cases} \theta_{rx}=\theta_{rz}=0,\ \theta_{py}=\theta_{pz}=0 \\ \omega_{rx}=\omega_{rz}=0,\ \omega_{py}=\omega_{pz}=0 \\ \dot{\omega}_{rx} = \dot{\omega}_{rz}=0,\ \dot{\omega}_{py}=\dot{\omega}_{pz}=0 \end{cases} \quad \text{(a2.6)}$$

So (a2.5) can be simplified into

$$\begin{cases} T_{yx} = J_{yx}[\dot{\omega}_{px}\cos\theta_{yz} - \omega_{yz}\omega_{px}\sin\theta_{yz} + \omega_{yz}\omega_{ry}\cos\theta_{px}\cos\theta_{yz} + (\dot{\omega}_{ry}\cos\theta_{px} - \omega_{px}\omega_{ry}\sin\theta_{px})\sin\theta_{yz}] \\ -(J_{yy} - J_{yz})(\omega_{ry}\sin\theta_{px} + \omega_{yz})(\omega_{ry}\cos\theta_{px}\cos\theta_{yz} - \omega_{yz}\sin\theta_{yz}) \\ T_{yy} = J_{yy}[-\dot{\omega}_{px}\sin\theta_{yz} - \omega_{yz}\omega_{rx}\cos\theta_{yz} - \omega_{yz}\omega_{ry}\cos\theta_{px}\sin\theta_{yz} + (\dot{\omega}_{ry}\cos\theta_{px} - \dot{\theta}_{px}\omega_{ry}\sin\theta_{px})\cos\theta_{yz}] \\ -(J_{yz} - J_{yx})(-\omega_{ry}\sin\theta_{px} + \omega_{yz})(\omega_{ry}\cos\theta_{px}\sin\theta_{yz} + \omega_{yz}\cos\theta_{yz}) \\ T_{yz} = J_{yz}(-\omega_{ry}\sin\theta_{px} - \omega_{px}\omega_{ry}\cos\theta_{px} + \dot{\omega}_{yz}) \end{cases}$$

(a2.7)